A Channel Drop Filter Using a Single Defect in a 2-D Photonic Crystal Slab—Defect Engineering With Respect to Polarization Mode and Ratio of Emissions From Upper and Lower Sides

Takashi Asano, Masamitsu Mochizuki, Susumu Noda, *Member, IEEE*, Makoto Okano, and Masahiro Imada

Abstract—A detailed theoretical analysis of defect engineering in a channel drop filter consisting of a single point defect near a waveguide in a two-dimensional (2-D) photonic crystal (PC) slab is presented. Initially, engineering of the point defect to control the polarization modes of emitted light is examined. By introducing an elliptical defect laterally shifted from the PC lattice, a single linearly polarized light mode can be selected to emit the majority of light, whereas light emitted from the original circular defect is made up of a range of linearly polarized modes. It is also shown that the ratio of light emitted from the top and bottom side of the defect can be improved considerably by introducing a defect with a stepped section along the vertical axis, thereby increasing the net efficiency of the device.

Index Terms—Dropping efficiency, nano-cavity, optical filter, photonic crystal (PC), polarization control, vertical asymmetry.

I. INTRODUCTION

PHOTONIC CRYSTALS (PCs), which are materials consisting of periodically varying refractive index, have received a lot of attention as a new type of optical material [1]–[12]. The main feature of PCs is their ability to form a photonic bandgap (PBG) when appropriate geometry is selected. In addition, defect states can be formed in the PBG by fabricating artificial defects in the crystal. By utilizing such defect states, various functional devices and/or applications are expected to be realized.

Recently, the trapping and emission of photons by a single point defect artificially introduced near a line defect waveguide in a two-dimensional (2-D) PC slab has been proposed and demonstrated [9], [13], [14]. The phenomenon of photons propagating along the waveguide being resonantly trapped by the point defect and emitted to free space is physically very interesting and is attractive for application to ultrasmall channel add/drop filtering or wavelength monitoring devices. Wavelength tunability and light dropping efficiency are very important in these devices. Filtering wavelength has been

The authors are with the Department of Electronic Science and Engineering, Kyoto University, Kyoto 606-8501, Japan, and with CREST, Japan Science and Technology Corporation, Kyoto 606-8501, Japan (e-mail: tasano@qoe.kuee.kyoto-u.ac.jp; snoda@kuee.kyoto-u.ac.jp).

successfully controlled by tuning the radius of an enlarged air hole defect in a 2-D PC slab consisting of a triangular array of air holes [9], [13], [14]. The theoretical maximum light dropping efficiency of the device has been found to be 50% [13], [14] in the case of a single point defect. It is thought that efficiency can be improved to almost 100% using cascaded defects [6], [15]. However, half of the light dropped from the waveguide is emitted from the upper side of the slab, while the other half is emitted from the lower side due to vertical symmetry of the structure. It has also been found that light emitted from the defect is largely unpolarized due to in-plane symmetry of the circular defect. For practical applications, the coupling efficiency between the point defect and external optical components strongly depends on polarization of the light. For some applications, linearly polarized light is more useful than unpolarized light and, hence, polarization tuning is necessary.

An attempt to design defect structures that improve the characteristics of the emitted light, i.e., defect engineering, is presented. First, it is demonstrated theoretically and experimentally that the polarization mode can be tuned by reducing symmetry of the defect. It is also shown theoretically that the ratio of light emitted from upper and lower sides can be improved dramatically by introducing vertical asymmetry into the defect structure. It is thought that high-performance channel add/drop filtering devices can be realized by combining these methods.

II. BASIC OPERATION MECHANISM

A. Device Structure and Defect Frequency

Fig. 1(a) shows schematically the basic structure of the surface-emitting channel drop filtering devices under consideration, which are based on 2-D PC slabs consisting of a triangular lattice of air holes. Air hole radii, slab thickness, and refractive index of the slabs were chosen to be $0.29\,a$, $0.6\,a$, and 3.4, respectively, where a is the lattice constant of the PC. A line defect in the form of a row of missing air holes along Γ–J direction is introduced into the PC forming a waveguide, with a single point defect in the form of an enlarged air hole created nearby. All calculations in this paper were carried out using three-dimensional (3-D) finite-difference time-domain (FDTD) methods [16], [17], with only transverse electric (TE)-like modes considered. A photonic bandgap appears
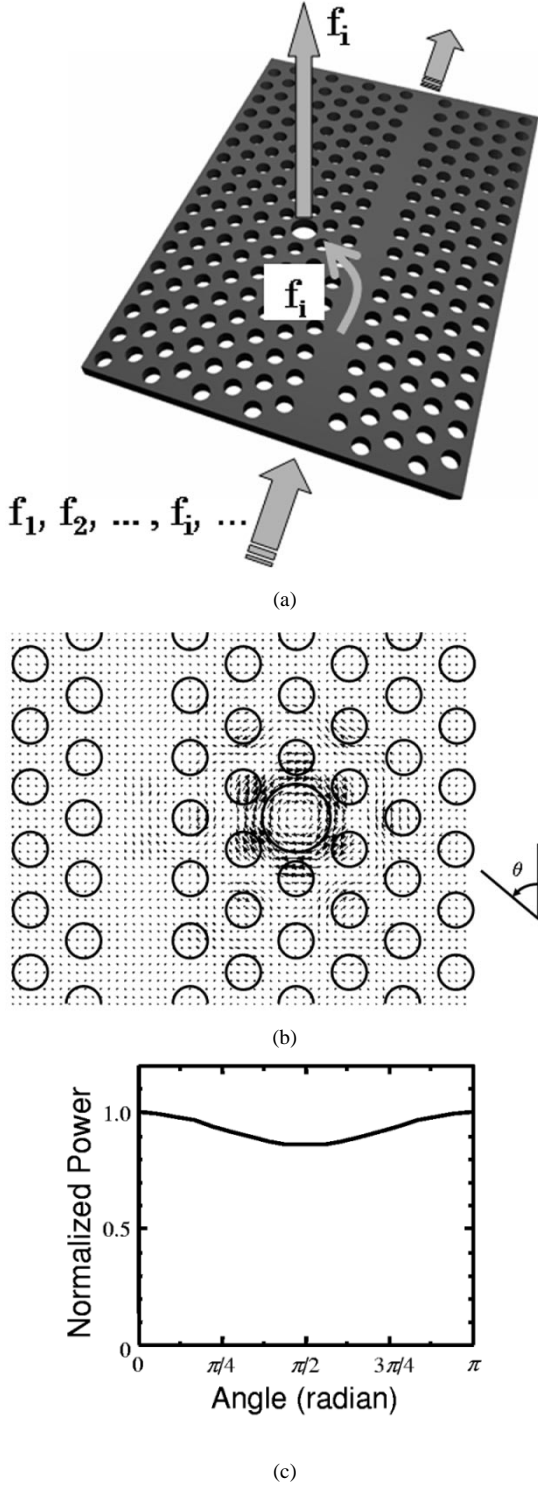
(a)

(b)

(c)

Fig. 1. (a) Schematic of 2-D PC slab with a line defect waveguide and a single point defect. Photons propagating along the waveguide are trapped and emitted to free space when photon frequency matches the frequency of defect modes. (b) Vector-field pattern of the fundamental defect-mode electric field across the center plane of the slab of a circular acceptor defect with a radius of 0.56 a. Circles indicate air rods in the dielectric slab. Polarization angle θ, which is defined as the angle between the waveguide and the electric field of the polarized light, is shown in the inset. (c) Power of polarized radiation dropped from the circular PC defect as a function of polarization angle (θ). Power is summed over all solid angles.

in the frequency range 0.256 to 0.320 c/a, with single and nonleaky waveguide modes forming in the frequency region

0.27 ∼ 0.28 c/a. The frequency of an acceptor defect increases from 0.27 to 0.28 c/a when the defect radius is increased from 0.55 to 0.58 a. A detailed band structure of the device is shown in [13] and [14].

B. Mode Field of Circular Point Defect

The electric-field distribution of a fundamental defect mode in a circular acceptor defect with a radius of 0.56 a is shown in Fig. 1(b). It can be seen that the electric field is hexagonal symmetry and is almost concentric with the defect air hole. The electric field is localized around the circumference of the defect and reflects the electric field of a slab with no defect. Removal of the dielectric pushes the mode frequency up into the PBG, and the field of the mode becomes localized around the defect due to confinement by the PBG. Because of the hexagonally symmetric of the mode field, it would seem that light emitted from the defect could not be totally linearly polarized. In order to calculate polarization characteristics, the power of radiation from the defect for each polarization angle was calculated. An observation plane parallel to the slab and a distance of 4.2 a from it is assumed. Power was obtained by integrating all Poynting vectors that cross the plane after filtering out specific polarization components. Time integration was also carried out over a time span of about 75 electromagnetic-field oscillations. Power radiated as a function of polarization direction is shown in Fig. 2(b). In this paper, polarization direction θ represents the angle between electric field and waveguide direction, as shown in the inset of Fig. 1(b). As expected, Fig. 1(c) shows that the light is largely unpolarized, although a drop in intensity at around a polarization angle of $\pi/2$ is observed due to circular symmetry of the device being broken by the waveguide. (In fact, polarization characteristics were found to depend on the collection angle of the Poynting power vectors. For example, it was found that radiation emitted perpendicularly from the circular defect is almost totally linearly polarized in the $\theta = \pi/2$ direction [18]. However, we limit our investigation to the polarization characteristics of total radiation to keep the results general.)

III. DEFECT ENGINEERING

A. Polarization-Mode Control

As mentioned in Sections I and II, circular defects that do not emit linearly polarized light due to their symmetry have been studied previously. The first attempt to produce linearly polarized light was the use of elliptical defects to reduce in-plane symmetry. As a circular defect is gradually transformed into an elliptical defect, electric flux near the vertices of the ellipse begins to cross the interface between the defect and the surrounding dielectric [see Fig. 2(a), (b), and (c)]. Due to the continuity of electric field and dielectric flux at the interface [see Fig. 2(b)], electric field in the defect becomes larger than in the surrounding dielectric. Therefore, the electric field near the vertices of the ellipse, which are the very regions where dielectric was removed to form the defect shape, is expected to get stronger.

The electric-field distribution of an elliptical defect having a minor to major axis ratio of 0.8 and an average radius of 0.56 a [the same as shown in Fig. 1(b) and (c)] was calculated and is
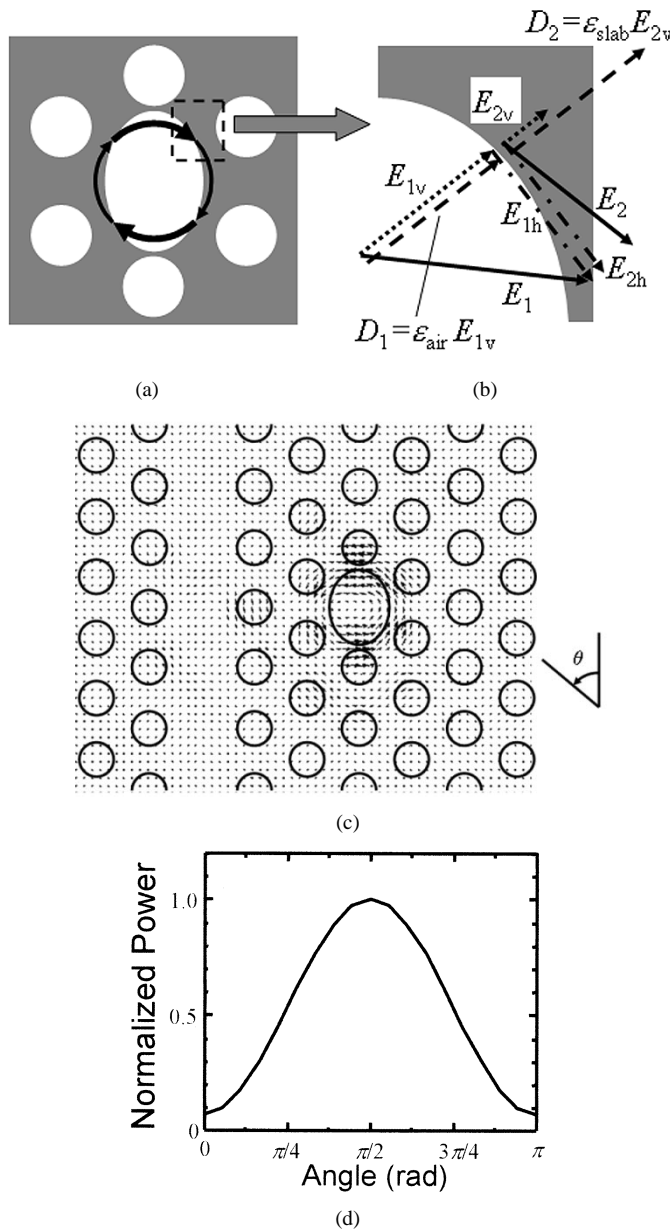
Fig. 2. (a) Schematic of an elliptical acceptor defect showing the main electric-field component of the defect mode. (Shading indicates dielectric material, arrows indicate electric flux.) (b) Enlargement of the vertex of the elliptical defect shown in (a), illustrating continuity of electric flux across the interface between air and dielectric material. Broken and dotted lines correspond to dielectric flux and electric-field vectors perpendicular to the interface (D_v, E_v, respectively). ε_{air} and ε_{slab} represent dielectric constants of air and slab materials. Dash-dotted lines represent electric-field vector parallel to the interface (E_h). Solid lines are sum of perpendicular and parallel electric-field vectors. Subscript 1 indicates vectors within the defect, while subscript 2 indicates vectors outside the defect. (c) Vector-field pattern of the fundamental defect-mode electric field across the center plane of the slab of an elliptic acceptor defect. Ratio of major to minor axis is 0.8, while the average radius is 0.56 a. Polarization angle (θ) is shown in the inset. (d) The power of polarized radiation dropped from the elliptical PC defect as a function of polarization angle (θ). Power is summed over all solid angles.

shown in Fig. 2(c). It can be seen that electric field is localized near the vertices. The polarization characteristics of the emitted radiation were also calculated and are shown in Fig. 2(d). It can be seen that light emitted from the defect is almost totally linearly polarized at an angle of $\pi/2$. The degree of linear polarization was evaluated by taking the ratio of the power of light po-

larized in the direction with the maximum power to that of light polarized in the orthogonal direction. For the elliptic defect, this ratio is 1:0.1, which is much higher than that of the circular defect (about 1 : 0.85). However, polarization of the light is not perfect, with the components of light polarized orthogonally to the primary polarization direction accounting for around 10% of total power emitted.

To obtain more complete polarization, the elliptical defect was shifted relative to the original lattice point. By shifting the ellipse along the major axis, it was thought that the electric-field flux crossing the defect edge could be confined to the vertex in the direction of the shift. As a result, a strong electric field is expected at this vertex. Fig. 3 shows theoretical results for an elliptical defect with the same shape as in Fig. 2, but shifted 0.05 a [Fig. 3(a)] relative to its original location. It can be seen in Fig. 3(b) that the electric field is strongly concentrated as predicted. The degree of polarization is greater than 1 : 0.01, as can be seen in Fig. 3(c). Although various shifting distances were tried, 0.05 a was found to give the best polarization. Polarization degree drops for shifts of less than 0.05 a, while for shifts larger than 0.05 a, electric-field concentration occurs not only within the vertex, but also in the dieletric material on either side of the vertex, where the distance to neighboring air holes is reduced. Having the electric field concentrated in three points instead of one reduces the degree of polarization.

A sample device containing an elliptical defect with a lateral shift was fabricated using the method reported in [14]. Light was injected into the waveguide from a facet, and the intensity of light emitted from the point defect at different polarizations was measured using a polarizer. Experimental results are shown in Fig. 4(a) and (b), clearly indicating that almost total linear polarization is achieved experimentally using the given defect geometry.

Because principles behind the demonstrated electric-field concentration were thought to be independent of the direction of shift, it was thought that polarization angle could be tuned arbitrarily by shifting in different directions. Rotated elliptical defects, in which the major axis was no longer parallel to the waveguide, were introduced as shown in Fig. 5(a). The polarization characteristics of light emitted from defects with different rotation angles (φ) are shown in Fig. 5(b). It can be seen that in every case, linearly polarized light was emitted and that the polarization angle (θ) changed as the rotation angle (φ) changed. The relationship between polarization angle (θ) and defect rotation angle (φ) was extracted from Fig. 5(b) and is plotted in Fig. 5(c), demonstrating that polarization angle can be tuned to any value in the range $0 \sim 60°$ by appropriate selection of ellipse orientation. These results are sufficient to demonstrate the tuning of polarization to an arbitrary direction given the near hexagonal symmetry of the PC structure. [The device structure is not truly hexagonally symmetric because of the existence of the waveguide. However, the influence of the waveguide on the symmetry of the point defect mode is thought to be much weaker than the influence of the shape of the ellipse itself, which is supported by the fact that polarization direction is a function of defect rotation angle, as shown in Fig. 5(c).]

Next, the effects of defect geometry perturbations (shape, position, and rotation) on defect characteristics other than polar-
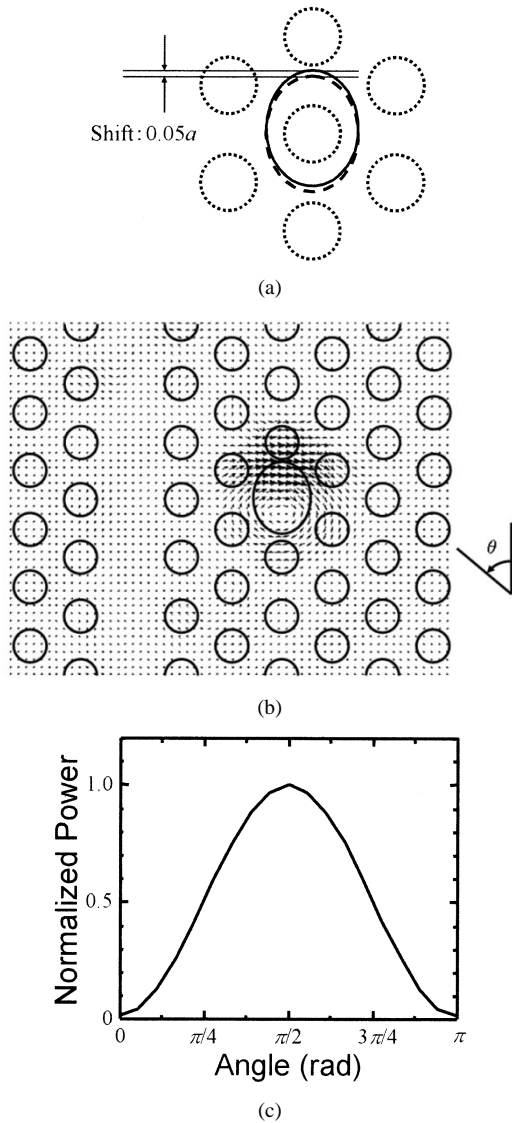
(a)

(b)

(c)

Fig. 3. (a) Schematic of an elliptical defect that has been shifted along the major axis (solid line). Ratio of major to minor axis is 0.8, average radius is 0.56 a, and shift is 0.05 a. The dotted circle shows the original air rod position, while the dotted ellipse shows the elliptical defect prior to shifting. (b) Vector-field pattern of the fundamental defect-mode electric field across the center plane of the slab shown in (a). The polarization angle (θ) is shown in the inset. (c) The power of polarized radiation dropped from the defect as a function of polarization angle (θ). Power is summed over all solid angles.

ization were examined. In all cases, changes in the resonant frequency of the defect were extremely small (deviations from the frequency of a circular defect were less than 3%). However, Q factors of the shifted elliptical defects were much smaller. In the case of Fig. 1(b) (circular) and 2(b) (elliptic but not shifted), integrating electric field over the slab plane gives almost zero due to the symmetry of the field. This means that emission of light perpendicular to the slab is nearly prohibited because the electric field cancels itself out. In contrast, in the case of Fig. 3(b) (elliptic and shifted defect), in-plane electric fields do not cancel out, because the electric field is concentrated around one vertex of the ellipse. Therefore, light emissions in the perpendicular direction are allowed, and the Q factor of the cavity decreases due to the increase in radiation loss. Vertical Q (which is a function of radiation loss) of the shifted elliptic defect shown in Fig. 3 is
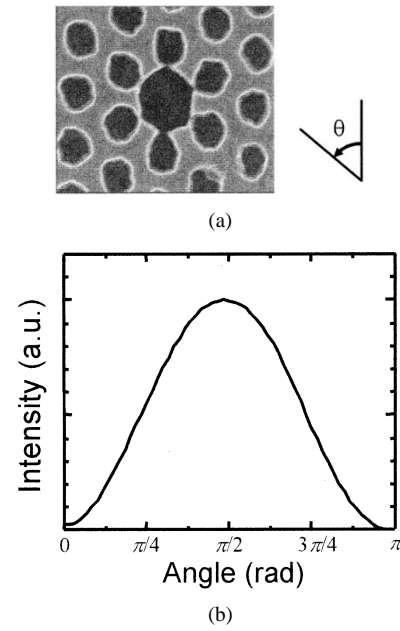

(a)

(b)

Fig. 4. (a) Scanning electron microscope image of the fabricated shifted elliptic acceptor defect. The lattice constant (distance between nearest neighbor air holes) is 0.42 μm. The fabricated structure contains a line-defect waveguide as well as the point defect, however, only an image of the point defect is presented. The waveguide is oriented vertically with respect to the image. (b) Experimentally measured power as a function of polarization angle (θ). Radiated light was collected using an objective lens with a numerical aperture of 0.4.

about one-fifth of that of the circular defect. We think that the Q factor can be recovered to some extent by tuning the radius of the defect [14]. The dropping efficiency also decreases because the relationship between in-plane Q (which is determined by coupling to the waveguide mode) and vertical Q deviates from optimum [13], [14]. However, this can be compensated for by changing the distance between the point defect and the waveguide to help restore dropping efficiency [13], [14].

B. Control of Emission Ratio of Upper to Lower Sides

As mentioned in Section I, when using a vertically uniform defect, the ratio of emissions from the upper and lower sides (referred to as η_v) is 1 and, hence, net efficiency is halved. To address this, vertically nonuniform defects were examined. A cross section of the electric field calculated for a vertically uniform defect (radius 0.56 a) is shown in Fig. 6. Because of the Fresnel–Kirchhoff diffraction integral and Sommerfeld's radiation condition, the intensity of radiation is expected to depend on the electromagnetic field near the surface of the slab. By the conservation of wavevectors parallel to the slab, only electromagnetic-field components that have an in-plane wavevector shorter than that in the free space can be radiated from the surface [19]. As can be seen in Fig. 6(a), the period of the main electric-field oscillation in the defect mode along the slab is 1/3~1/4 of the wavelength of light at the defect frequency in a vacuum. This means that the main defect-mode component does not radiate because it has an in-plane wavevector much larger than that in vacuum.

In this case, the effect of an envelope function that overlaps the main oscillation component is important. For an envelope function that is highly localized or varies rapidly, the Fourier
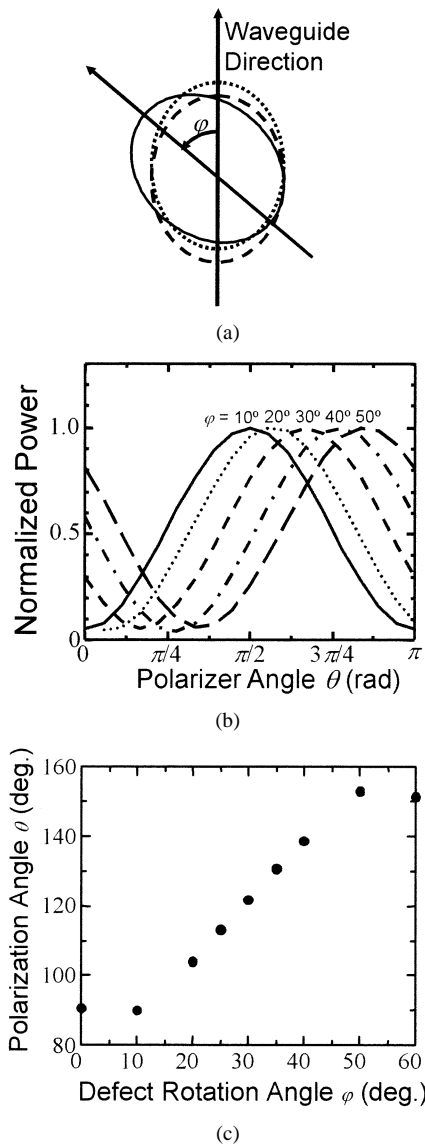
Fig. 5. (a) Schematic of an elliptical defect shifted along the major axis and rotated by φ from the original direction (solid line). The broken line shows the defect prior to shifting from the original lattice point. The dotted line shows a shifted elliptical defect without rotation. (b) Power as a function of polarization angle (θ) for defects rotated φ. Power is summed over all solid angles. (c) Polarization angle (θ) as a function of ellipse rotation angle (φ).

Fig. 6. (a) Top view of the refractive-index distribution of a cylindrical defect. (b) Cross- section of electric field along the dashed line shown in (a). Intensity of the electric field perpendicular to the plane is represented by colors. A horizontal bar illustrates the wavelength of light in a vacuum whose frequency corresponds to the defect frequency.

transformation of the envelope function contains a broad range of wavevector components. The electric-field pattern of the defect mode in wavevector space is determined by convolution of the Fourier transformed main oscillation component (delta function) with the Fourier transformed envelope function. Therefore, the in-plane wavevector of the defect mode becomes uncertain, with the possible range of wavevectors broadened by localizations or rapid changes in the envelope function. If this effect is strong enough, the defect mode comes to have components with wavevectors smaller than those in vacuum, and it is through these electromagnetic field components that radiation is allowed [20]. We believe that the electromagnetic field near the edge of the defect air hole, as shown in Fig. 6(b), can be shifted slightly to the upper side of the slab by introducing some kind of vertical asymmetry. The electric field at the upper side of the slab would then become strongly spatially localized near the defect,
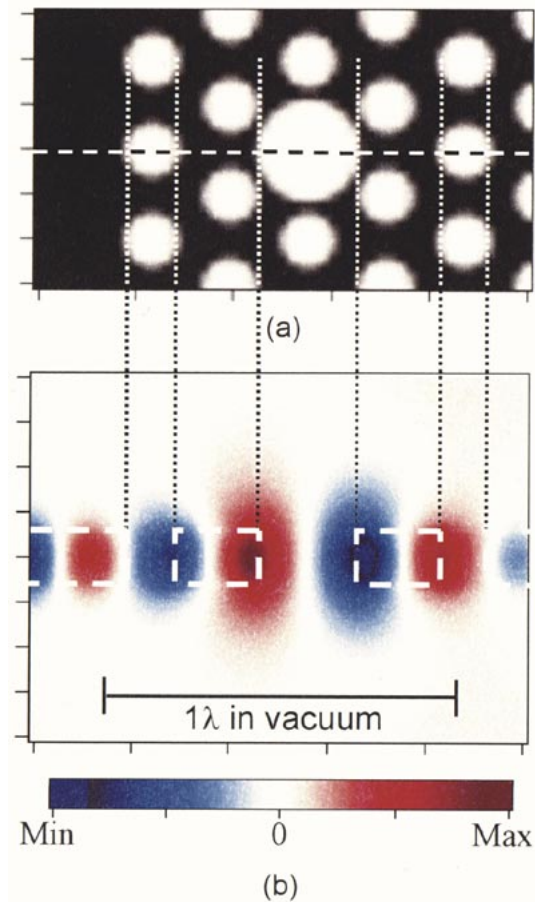
while being uniform along the in-plane direction at the lower side. This would lead to an increase in emissions from the upper side and suppression of emissions from the lower side.

To test this idea, a stepped defect was introduced into the enlarged air hole, with the step located in the middle of the slab, as shown in Fig. 7(a). It was thought that such a structure would shift the electromagnetic field to the upper side, because electromagnetic waves are confined vertically by refractive-index contrast and the average refractive index is higher in the upper side. Electric-field distribution and emission ratio η_v were calculated. The difference in radius between the upper half of the air rod and the lower half is defined as Δr, while average air rod radius is the same as in the original defect ($0.56\ a$). The cross section of the electric-field distribution of a defect with $\Delta r = 0.20\ a$ was calculated for such structures and is shown in Fig. 7(b). This shows that the electromagnetic field becomes localized in the upper side of the defect by the asymmetry. Fig. 7(c) shows the relationship between η_v and Δr. It can be seen that emission ratio η_v increases with Δr due to increasing differences in refractive index between the upper and lower side of the slab. It can also be seen that emission ratios as high as 15:1 can be obtained, improving the net output efficiency of the channel drop filter considerably. (Calculations for $\Delta r > 0.25\ a$ were also conducted but were thought to be unreliable, because reflections

from the upper absorption boundary could not be ignored for lower side emissions.)

Effects of vertically asymmetric defect geometry on defect performance characteristics other than emission ratio were also calculated. Changes in the resonant frequency of the defect were small, with deviations from the original defect frequency of less than 1%. Vertical Q of the defect decreases as Δr increases, dropping to one-third of that of the symmetric defect when Δr is 0.25. However, we believe that this could be counteracted to some extent by reducing the spatial localization of the electromagnetic field by changing the size of the defect [14]. The relationship between in-plane Q and vertical Q, which determines the dropping efficiency, can be also restored by tuning the distance between the point defect and waveguide [13], [14]. In addition, we have noticed that vertically asymmetric structures give rise to the excitation of transverse magnetic (TM)-like modes in a PC slab [21]. However, these effects are complicated and will be presented in a separate publication.

IV. CONCLUSION

Point defect modes of channel drop filters in 2-D PC slab were analyzed in order to find ways to control fundamental characteristics of the emitted light. First, operational principles of the device and electric-field distributions of defect modes were determined for a circular defect. Next, defect engineering was explored with respect to polarization modes of emitted light. It was found that light emitted from the circular defect is largely unpolarized due to the PC hexagonal symmetry. By introducing an elliptical defect shifted along the major axis with respect to the PC lattice, this symmetry could be reduced, resulting in the emission of almost totally linearly polarized light. Results were confirmed experimentally. It has also been shown theoretically that polarization direction can be tuned to an arbitrary direction by rotating the elliptical defect. Tunability of the polarization mode would be very useful for coupling between the device and external optical components. Finally, defect engineering was explored with respect to the ratio of light emitted from the upper and lower sides of the defect. By introducing a defect with a stepped section along the vertical axis, upper-to-lower-side emission ratios as high as 15:1 were obtained, improving the net efficiency of the device considerably. These results indicate that precise defect engineering is indispensable in realizing highly functional optical devices based on defects in 2-D PCs designed for application to wavelength-division-multiplexing optical communication systems, such as our ultrasmall channel drop filters.
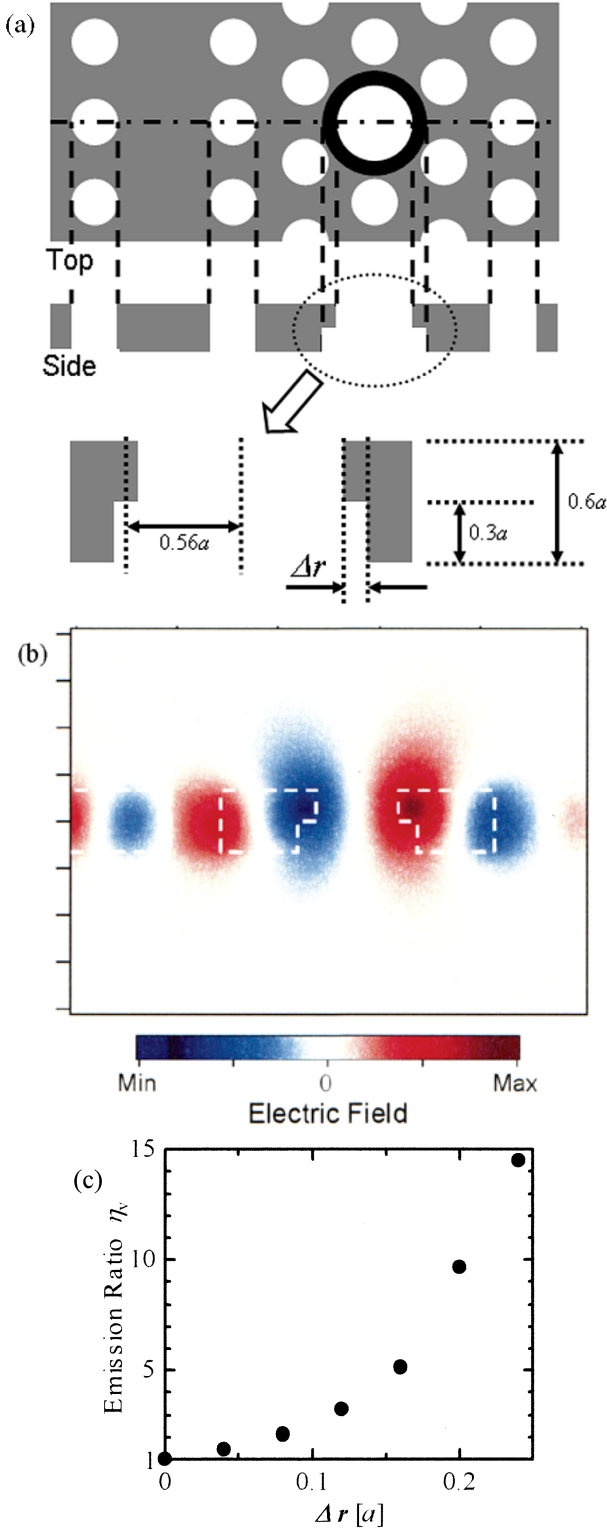

Fig. 7.   (a) Schematic of a stepped defect showing top view (upper) and cross-sectional side view (middle). The cross-sectional plane is indicated by the horizontal dash-dotted line in the top view. The expanded side view (lower) shows structural parameters. The radius of the upper circle is Δr smaller than that of the lower circle, with the average radius of 0.56 a. The step is located midway across the slab. (b) Electric field along the cross-sectional plane shown in (a) for the $\Delta r = 0.20\ a$ case. The intensity of the electric-field perpendicular to the plane is represented by colors. The dashed white line shows the boundary between slab material and air. (c) Ratio of emissions from upper and lower side (η_v) as a function of the difference between upper and lower radii (Δr) calculated for the stepped defect shown in (a).

REFERENCES

[1] E. Yablonovitch, "Photonic band-gap structures," *J. Opt. Soc. Amer. B*, vol. 10, pp. 283–295, 1993.

[2] S. John, "Localization of light," *Phys. Today*, pp. 32–40, May 1991.

[3] A. Mekis, J. C. Chen, I. Kurland, S. Fan, P. R. Villeneuve, and J. D. Joannopoulos, "High transmission through sharp bends in photonic crystal wave guides," *Phys. Rev. Lett.*, vol. 77, pp. 3787–3790, 1996.

[4] S. Noda, N. Yamamoto, and A. Sasaki, "New realization method for three dimensional photonic crystal waveguides," *Jpn. J. Appl. Phys.*, vol. 35, pp. L909–L912, 1996.

[5] J. D. Joannopoulos, P. R. Villeneuve, and S. Fan, "Photonic crystals: Putting a new twist on light," *Nature*, vol. 386, pp. 143–149, 1997.

[6] S. Fan, P. R. Villeneuve, J. D. Joannopoulos, and H. A. Haus, "Channel drop tunneling through localized states," *Phys. Rev. Lett.*, vol. 80, pp. 960–963, 1998.

[7] S. Y. Lin, J. G. Fleming, D. L. Hetherington, B. K. Smith, R. Biswas, K. M. Ho, M. M. Sigalas, W. Zubrzycki, S. R. Kurtz, and J. Bur, "A three-dimensional photonic crystal operating at infrared wavelengths," *Nature*, vol. 394, pp. 251–253, 1998.

[8] O. Painter, J. Vuckovic, and A. Scherer, "Defect modes of a two-dimensional photonic crystal in an optically thin dielectric slab," *J. Opt. Soc. Amer. B*, vol. 16, pp. 275–285, 1999.

[9] S. Noda, A. Chutinan, and M. Imada, "Trapping and emission of photons by a single defect in a photonic bandgap structure," *Nature*, vol. 407, pp. 608–610, 2000.

[10] S. Noda, K. Tomoda, N. Yamamoto, and A. Chutinan, "Full three-dimensional photonic bandgap crystals at near-infrared wavelengths," *Science*, vol. 289, pp. 604–606, 2000.

[11] A. Chutinan and S. Noda, "Waveguides and waveguide bends in two-dimensional photonic crystal slabs," *Phys. Rev. B*, vol. 62, pp. 4488–4492, 2000.

[12] S. Noda, M. Yokoyama, M. Imada, A. Chutinan, and M. Mochizuki, "Polarization mode control of two-dimensional photonic crystal laser by unit cell structure design," *Science*, vol. 293, pp. 1123–1125, 2001.

[13] A. Chutinan, M. Mochizuki, M. Imada, and S. Noda, "Surface-emitting channel drop filters using single defects in two dimensional photonic crystal slabs," *Appl. Phys. Lett.*, vol. 79, pp. 2690–2692, 2001.

[14] M. Imada, S. Noda, A. Chutinan, M. Mochizuki, and T. Tanaka, "Channel drop filter using a single defect in a 2-D photonic crystal slab waveguide," *IEEE J. Lightwave Technol.*, vol. 20, pp. 873–878, May 2002.

[15] C. Manolatou, M. J. Khan, S. Fan, P. R. Villeneuve, H. A. Haus, and J. D. Joannopoulos, "Coupling of modes analysis of resonant channel add-drop filters," *IEEE J. Quantum Electron.*, vol. 35, pp. 1322–1331, Sept. 1999.

[16] K. S. Yee, "Numerical solution to initial boundary value problems involving Maxwell's equations in isotropic media," *IEEE Trans. Antennas Propagat.*, vol. AP-14, pp. 302–307, May 1966.

[17] G. Mur, "Absorbing boundary conditions for the finite-difference approximation of the time-domain electromagnetic-field equations," *IEEE Trans. Electromagn. Compat.*, vol. EMC-23, pp. 377–382, Nov. 1981.

[18] T. Asano, B. S. Song, Y. Tanaka, and S. Noda, "Investigation of a channel-add/drop-filtering device using acceptor type point defects in a two-dimensional photonic crystal slab," *Appl. Phys. Lett.*, submitted for publication.

[19] K. Sarinivasan and O. Painter, "Momentum space design of high-Q photonic crystal optical cavities," *Optics Express*, vol. 10, pp. 670–684, 2002.

[20] Y. Akahane, T. Asano, and S. Noda, "High-Q photonic nanocavity in two-dimensional photonic crystal slabs," , (unpublished).

[21] Y. Tanaka, T. Asano, Y. Akahane, and S. Noda, "Theoretical investigation of a two-dimensional photonic crystal slab with tapered air holes," *Appl. Phys. Lett.*, vol. 82, no. 9, pp. 1661–1663, Mar. 2003.

Takashi Asano, photograph and biography not available at the time of publication.

Masamitsu Mochizuki, photograph and biography not available at the time of publication.

Susumu Noda (M'92), photograph and biography not available at the time of publication.

Makoto Okano, photograph and biography not available at the time of publication.

Masahiro Imada, photograph and biography not available at the time of publication.